Smart Structures and Systems, *Vol. 18, No. 2 (2016) 355-374*
DOI: http://dx.doi.org/10.12989/sss.2016.18.2.355

Transverse dynamics of slender piezoelectric bimorphs with resistive-inductive electrodes

Juergen Schoeftner*[1], Gerda Buchberger[2a] and Ayech Benjeddou[3b]

[1]*Johannes Kepler University, Institute of Technical Mechanics, Altenbergerstrasse 69, 4040 Linz, Austria*
[2]*Johannes Kepler University, Institute of Biomedical Mechatronics, Altenbergerstrasse 69, 4040 Linz, Austria*
[3]*SUPMECA, 3 rue Fernand Hainaut, 93407 Saint Ouen CEDEX, France*

(Received October 19, 2016, Revised March 8, 2016, Accepted March 23, 2016)

Abstract. This paper presents and compares a one-dimensional (1D) bending theory for piezoelectric thin beam-type structures with resistive-inductive electrodes to ANSYS® three-dimensional (3D) finite element (FE) analysis. In particular, the lateral deflections and vibrations of slender piezoelectric beams are considered. The peculiarity of the piezoelectric beam model is the modeling of electrodes in such a manner that is does not fulfill the equipotential area condition. The case of ideal, perfectly conductive electrodes is a special case of our 1D model. Two-coupled partial differential equations are obtained for the lateral deflection and for the voltage distribution along the electrodes: the first one is an extended Bernoulli-Euler beam equation (second-order in time, forth order in space) and the second one the so-called Telegrapher's equation (second-order in time and space). Analytical results of our theory are validated by 3D electromechanically coupled FE simulations with ANSYS®. A clamped-hinged beam is considered with various types of electrodes for the piezoelectric layers, which can be either resistive and/or inductive. A natural frequency analysis as well as quasi-static and dynamic simulations are performed. A good agreement between the extended beam theory and the FE results is found. Finally, the practical relevance of this type of electrodes is shown. It is found that the damping capability of properly tuned resistive or resistive-inductive electrodes exceeds the damping performance of beams, where the electrodes are simply linked to an optimized impedance.

Keywords: piezoelectric effect; conductive electrodes; linear piezoelectric beam and bar modeling; passive vibration control; bending vibration; finite element analysis

1. Introduction

Intelligent structures are systems with multi-functional materials, which manipulate the motion in a desired manner. One possibility to influence the structure is based on the piezoelectric effect, either by feedforward or feedback control of the piezoelectric control devices (actuation) or by dissipation of the electric energy (passive control), which then affects the motion of the host structure. An overview of the research domain of adaptronics, where the piezoelectric effect is

*Corresponding author, Ph.D., E-mail: juergen.schoeftner@jku.at
[a] Ph.D. Student, Email: gerda.buchberger@jku.at
[b] Professor, E-mail: ayech.benjeddou@supmeca.fr

http://www.techno-press.org/?journal=sss&subpage=8 ISSN: 1738-1584 (Print), 1738-1991 (Online)

only one of many others used for measuring physical quantities or for the control of structures, is given by Janocha (2007). Classical and introductory works on piezoelectricity are Crawley (1994), Chopra (2002) and Tzou (1998). For the particular use of piezoelectric transducers or patches, the reader is referred to the books by Moheimani and Fleming (2006) and Preumont (2006), where the focus is laid on the reduction of structural vibrations.

The concept of passive vibration control is referred to Forward (1979), who was the first to attenuate vibrations of an optical device by linking the piezoelectric transducer to an external circuit. This circuit was replaced by resistive-inductive impedances in Hagood and Flotow (1991), which then opened the field for single- and multi-mode shunt strategies and semi-passive control methods, e.g., Niederberger *et al.* (2004), Park (2003) and Trindade and Maio (2008). The experimental results of a shunt damped cantilevered plate from Hagood and Flotow (1991) are used by Thornburgh and Chattopadhyay (2002) to verify their finite element (FE) model. Contrary to most electromechanically coupled FE formulations, they used the electrical displacement field instead of the electric potential as the electrical degree of freedom (DOF). Later they used this formulation to develop an optimization procedure in order to calculate the parameters of an attached electrical circuit of a plate, see Thornburgh and Chattopadhay (2003). In Krommer and Irschik (2001) the authors investigated the influence of the electric field on transverse vibration of a simply-supported piezoelectric bimorph. A beam model was then developed by Krommer (2001), which properly takes into account indirect and direct piezoelectric effects within the framework of the Bernoulli-Euler theory. He also investigated the influence of short-, open-circuited and no electrodes on the deflection and on the eigenfrequencies. An extension to the Timoshenko beam theory is later given by Krommer and Irschik (2002). A piezoelectric beam theory for moderately thick structures (Timoshenko beam), where the electrodes of the piezoelectric layers are connected to external electric circuits, was presented in Schoeftner and Irschik (2011). This model was later used to derive conditions for passive shape control, see Schoeftner and Irschik (2011b): the width of the piezoelectric layers and the impedance of the electric circuit are computed, such that time-harmonic vibrations due to external loads are completely canceled. FE beam formulations for piezoelectric sandwich structures were derived in Benjeddou *et al.* (1997) and (1999). Based on the variational formulation of a sandwich beam, the differential equations are given in terms of mass and stiffness matrices and mechanical and electrical force vectors. Extension and shear actuation mechanisms are accounted for in this model. Static and dynamic analyses are performed for sandwich structures with a large or a small soft core and compared to literature.

In contrast to metal electrodes, polymer electrodes cause a significant potential loss over the electrode surface, e.g. position-sensitive touchpads exploit this fact in order to detect the location of a pressure source, see Buchberger *et al.* (2008, 2008b). A model properly coupling mechanical assumptions, the piezoelectric effect and resistive electrodes has been published first by Lediaev (2010), who analyzed the interaction of moderately and low conductive electrodes with three-dimensional (3D) vibrations of a cantilever. Buchberger and Schoeftner (2013) combined elementary beam theory, piezoelectricity and resistive electrodes to obtain an extended beam differential equation, which is coupled to a diffusion equation for the electric potential of the electrodes. It has been shown that shape control can be realized by properly tuning the electrode resistance, see Schoeftner *et al.* (2014). The practical application of the innovative control method is proven by the issued patent (Schoeftner and Buchberger 2013) and the experimental realization (Schoeftner *et al.* 2015b).

In the following, first, the partial differential equations for a piezoelectric bimorph with resistive-inductive electrodes are recalled when the axial and lateral deflections are coupled.

Considering a symmetric bimorph, the axial motion can be dropped, yielding that the beam equation (forth-order in space, second-order in time) is coupled to the wave equation, which describes the electrodes (second order in space and time). Six boundary conditions are needed to solve the differential equations: four of them are denoted as mechanical boundary conditions, the remaining two are electrical ones. The one-dimensional (1D) extended beam model is validated by a 3D ANSYS® FE model. A natural frequency analysis is performed as well as frequency responses due to harmonic excitations (quasi-static and dynamic). Finally, the practical relevance of resistive-inductive electrodes is pointed out.

2. Equations of motion of a slender bimorph with resistive-inductive electrodes

Assuming a bimorph with two identical piezoelectric layers and constant (i.e., no dependency on x-axis) geometrical and material properties, the two equations of motion for axial $u_0(x,t)$ and lateral $w_0(x,t)$ deflections are (for a detailed derivations, see Schoeftner *et al*. (2015))

$$M_u \ddot{u}_0(x,t) - K_{\mathrm{N}} u_{0,xx}(x,t) = q_x(x,t) + \tilde{e}_{31}^{\mathrm{p}} b_{\mathrm{p}} \left[V_{,x}^{\mathrm{l}}(x,t) + V_{,x}^{\mathrm{u}}(x,t) \right] \tag{1}$$

$$M_w \ddot{w}_0(x,t) + K_{\mathrm{M}} w_{0,xxxx}(x,t) = q_z(x,t) + \tilde{e}_{31}^{\mathrm{p}} z_{\mathrm{m\,p}} b_{\mathrm{p}} \left[V_{,xx}^{\mathrm{l}}(x,t) - V_{,xx}^{\mathrm{u}}(x,t) \right]. \tag{2}$$

These equations are coupled to the damped wave equation (=the Telegrapher's equation) for the voltage, which determines the potential difference $V^k(x,t)$ across the electrodes of the lower ($k=\mathrm{l}$) and the upper ($k=\mathrm{u}$) layers

$$\begin{aligned} &-V_{,xx}^k(x,t) + cr\dot{V}^k(x,t) + cl\ddot{V}^k(x,t) \\ &\qquad = \tilde{e}_{31}^{\mathrm{p}} b_{\mathrm{p}} \left\{ r\left[\dot{u}_{0,x}(x,t) - z_{\mathrm{m}k} \dot{w}_{0,xx}(x,t) \right] + l\left[\ddot{u}_{0,x}(x,t) - z_{\mathrm{m}k} \ddot{w}_{0,xx}(x,t) \right] \right\}. \end{aligned} \tag{3}$$

For the sake of completeness, the definitions of the axial K_{N}, bending stiffness K_{M} as well as mass per unit length $M_u = M_w$ and capacitance c per unit length are recalled in Eq. (A.1). The damped wave Eq. (3) is the same as that of a damped transmission line (Telegrapher's equation), see Buchberger *et al.* (2008b) or Marshall *et al.* (1996). It is influenced by the velocity and acceleration of the axial strain of each layer $u_{0,x}(x,t) \mp z_{\mathrm{m\,p}} w_{0,xx}(x,t)$ and by the resistance r and the inductance l per unit length of the electrode.

Here, we are only interested in the lateral deflection. From Eq. (3) one sees that the bending strain $z_{\mathrm{m\,p}} w_{0,xx}(x,t)$ causes only sign-reversed voltages $V(x,t) = V^{\mathrm{l}}(x,t) = -V^{\mathrm{u}}(x,t)$ for the upper and lower layers. Hence, the axial deflection $u_0(x,t)$ is not excited if the axial load is $q_x(x,t) = 0$ or by the opposite phase voltages, see Eq. (1). It follows from Eqs. (1)-(3) that the two coupled differential equations for bending dynamics are

$$M_w \ddot{w}_0(x,t) + K_{\mathrm{M}} w_{0,xxxx}(x,t) = q_z(x,t) + 2\tilde{e}_{31}^{\mathrm{p}} z_{\mathrm{mp}} b_{\mathrm{p}} V_{,xx}(x,t) \tag{4}$$

$$-V_{,xx}(x,t)+crV\dot{}\,(x,t)+clV\ddot{}\,(x,t)=-\tilde{e}_{31}^{\mathrm{p}}b_{\mathrm{p}}z_{\mathrm{mp}}\left[r\dot{w}_{0,xx}(x,t)+l\ddot{w}_{0,xx}(x,t)\right]. \tag{5}$$

Grounding the inner electrodes, $\phi(x,z=0,t)=0$, one finds a relation between the electric potential $\phi(x,z,t)$ inside the piezoelectric layers, the electrode voltage $V(x,t)$ and the deflection $w_0(x,t)$

$$\phi(x,z,t)=\pm\frac{V(x,t)}{h_{\mathrm{p}}}z+\frac{\tilde{e}_{31}^{\mathrm{p}}}{\tilde{\kappa}_{33}^{\mathrm{p}}}\left(\pm zz_{\mathrm{mp}}-\frac{z^2}{2}\right)w_{0,xx}(x,t). \tag{6}$$

The plus and minus signs in Eq. (6) hold for the lower and upper layers, respectively.

The current flow $i(x,t)$ on the external electrodes can be determined from the Kirchhoff voltage and current rules

$$ri(x,t)+l\frac{\mathrm{d}i}{\mathrm{d}t}(x,t)=-V_{,x}(x,t) \tag{7}$$

$$i_{,x}(x,t)=-\tilde{e}_{31}^{\mathrm{p}}z_{\mathrm{mp}}\dot{w}_{0,xx}(x,t)b_{\mathrm{p}}-c\dot{V}(x,t). \tag{8}$$

Assuming that the excitation load is time-harmonic $q_z=\hat{q}_z\mathrm{e}^{\mathrm{i}(kx+\omega t)}$, the solution must be also time-harmonic

$$\begin{pmatrix}w_0(x,t)\\V(x,t)\end{pmatrix}=\begin{pmatrix}\hat{w}\\\hat{V}\end{pmatrix}\mathrm{e}^{\mathrm{i}(kx+\omega t)}, \tag{9}$$

yielding

$$\begin{pmatrix}-M_w\omega^2+K_{\mathrm{M}}k^4 & 2\tilde{e}_{31}^{\mathrm{p}}z_{\mathrm{mp}}b_{\mathrm{p}}k^2\\ -\tilde{e}_{31}^{\mathrm{p}}b_{\mathrm{p}}z_{\mathrm{mp}}k^2\left(\omega r\mathrm{i}-\omega^2 l\right) & k^2-\omega^2 cl+\omega cr\mathrm{i}\end{pmatrix}\begin{pmatrix}\hat{w}\\\hat{V}\end{pmatrix}=\begin{pmatrix}\hat{q}_z\\0\end{pmatrix}. \tag{10}$$

Inverting this equation, the solution is

$$\begin{pmatrix}\hat{w}\\\hat{V}\end{pmatrix}=\frac{1}{\det}\begin{pmatrix}\left(k^2-\omega^2 cl+\omega cr\mathrm{i}\right) & -2\tilde{e}_{31}^{\mathrm{p}}z_{\mathrm{mp}}b_{\mathrm{p}}k^2\\ \tilde{e}_{31}^{\mathrm{p}}b_{\mathrm{p}}z_{\mathrm{mp}}k^2\left(\omega r\mathrm{i}-\omega^2 l\right) & \left(-M_w\omega^2+K_{\mathrm{M}}k^4\right)\end{pmatrix}\begin{pmatrix}\hat{q}_{\bar{z}}\\0\end{pmatrix} \tag{11}$$

where the determinant is

$$\det=\left(-M_w\omega^2+K_{\mathrm{M}}k^4\right)\left(k^2-\omega^2 cl+\omega cr\mathrm{i}\right)+2k^4\left(\tilde{e}_{31}^{\mathrm{p}}z_{\mathrm{mp}}b_{\mathrm{p}}\right)^2\left(\omega r\mathrm{i}-\omega^2 l\right). \tag{12}$$

For a given excitation frequency ω, six roots for the wave-number k_j can be computed by setting the determinant equal to zero. The final solution can be written in the form of

$\left(w_0, V\right)^T = \sum_{j=1}^{6}\left(\hat{w}_j, \hat{V}_j\right)^T \mathrm{e}^{\mathrm{i}(kx+\omega t)}$; so, 12 unknown coefficients $\hat{w}_1, \hat{w}_2, ..., \hat{w}_6$ and $\hat{V}_1, \hat{V}_2, ..., \hat{V}_6$ have to be determined. However, taking into consideration the second equation in (10), which gives a relation between $\hat{w}_j, \hat{V}_j$, only six unknowns remain. They are determined by prescribing four mechanical and two electrical boundary conditions (see next section).

3. Formulation of the boundary conditions

3.1 Mechanical boundary conditions

For the mechanical boundary conditions we assume the classical boundary conditions at $x = x^*$ (either hinged, clamped, free or locking of the rotation):

- free: $M(x^*, t) = 0, Q(x^*, t) = 0$
- hinged: $M(x^*, t) = 0, w_0(x^*, t) = 0$
- rotation locked: $Q(x^*, t) = 0, w_{0,x}(x^*, t) = 0$
- clamped: $w_0(x^*, t) = 0, w_{0,x}(x^*, t) = 0$

The bending moment $M(x,t)$ and the shear force $Q(x,t) = 0$ depend on an elastic and on an inelastic part, so (see e.g., Schoeftner *et al.* (2015) or Krommer (2001))

$$\begin{aligned} M(x,t) &= \underbrace{-K_{\mathrm{M}} w_{0,xx}(x,t)}_{\text{...elastic (=mechanical) part}} + \underbrace{2\tilde{e}_{31}^{\mathrm{p}} z_{\mathrm{mp}} b_{\mathrm{p}} V(x,t)}_{\text{...inelastic (=electrical) part}} \\ Q(x,t) = M_{,x}(x,t) &= \underbrace{-K_{\mathrm{M}} w_{0,xxx}(x,t)}_{\text{...elastic (=mechanical) part}} + \underbrace{2\tilde{e}_{31}^{\mathrm{p}} z_{\mathrm{mp}} b_{\mathrm{p}} V_{,x}(x,t)}_{\text{...inelastic (=electrical) part}}. \end{aligned} \tag{13}$$

3.2 Electrical boundary conditions

The term electrical boundary condition represents the fact in which manner the internal and external electrodes (of the lower and upper piezoelectric layers) at the edges of the beam are connected. Several possibilities are shown in Fig. 1. The boundaries can be divided into two groups: one for the case of actuation (Figs. 1(a) and 1(b)) and one for the case of sensing or passive applications (Fig.1c and d). According to Eq. (9), they must be formulated in terms of the displacement and the voltage, so that the coefficients $\hat{w}_j, \hat{V}_j$ (and hence the solution w_0, V) may be computed.

3.2.1 Electrical boundaries for actuation

Fig. 1(a) shows an electrically actuated beam so that the voltage at the left end is prescribed by V_0 and the right end is linked to an electric circuit

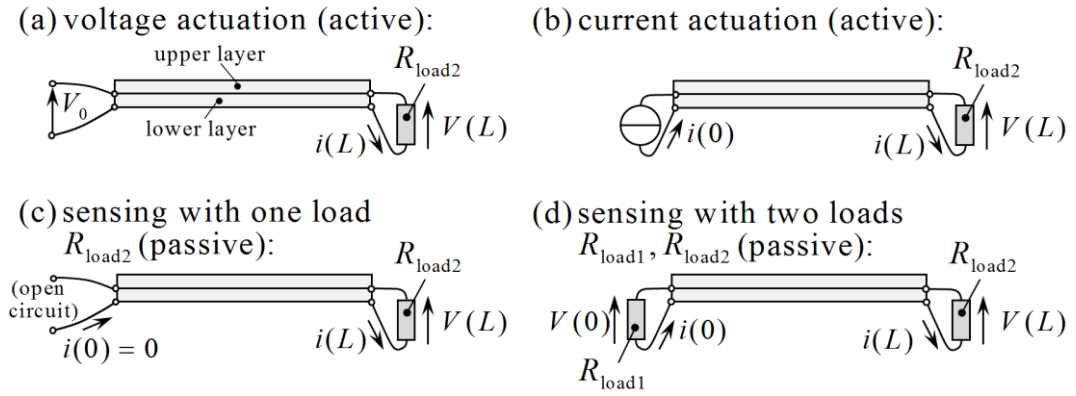

Fig. 1 Electrical boundary conditions, when (a) the voltage or (b) the current at the left end are prescribed; (c) electrodes remain unconnected (open-circuit) at the left end and connected by resistance at the right end; (d) both ends of the electrodes are connected by resistances. Note for reasons of simplicity the electric circuit is connected to the lower layer in the figure only

$$\begin{aligned} V(0) &= V_0 \\ R_{\text{load2}} i(L) &= V(L). \end{aligned} \tag{14}$$

According to Eq. (9), we need to express $i(L)$ in terms of the displacement and the voltage. E.g., when assuming resistive, but not inductive electrodes (i.e., $r \neq 0, l = 0$) and considering Kirchhoff's voltage rule Eq. (7) $V_{,x} / r = -i$, the second relation yields

$$V(L) = -R_{\text{load2}} \frac{V_{,x}(L)}{r}. \tag{15}$$

When the current is prescribed at the left boundary (Fig. 1(b)), one finds after inserting Eq. (7) and assuming $r \neq 0, l = 0$ again

$$\begin{aligned} i(0) = i_0 &\rightarrow V_{,x}(0) = i_0 r \\ R_{\text{load2}} i(L) = V(L) &\rightarrow -R_{\text{load2}} \frac{V_{,x}(L)}{r} = V(L). \end{aligned} \tag{16}$$

Eqs. (14) and (16) also include limit cases for the right boundary conditions: if the network is short-circuited $R_{\text{load2}} = 0$, the terminal voltage needs to be zero $V(L) = 0$. If it is open-circuited $R_{\text{load2}} \rightarrow \infty$, the electric current is $i(L) = 0$, and consequently the gradient of the voltage is also zero $V_{,x}(L) = 0$.

3.2.2 Electrical boundaries for sensing or passive applications

Two of the operation modes (e.g., if the piezoelectric layers are used as sensors) are depicted in Figs. 1(c) and 1(d). The case, when the electrodes are left open at one end (Fig. 1(c)), reads

$$\begin{aligned} &i(0)=0 \rightarrow V_{,x}(0)=0 \\ &V(L)=R_{\text{load}2}\,i(L) \rightarrow -R_{\text{load}2}\,\frac{V_{,x}(L)}{r}=V(L). \end{aligned} \tag{17}$$

Assuming the ends of the electrodes to be linked by two electric circuits (Fig. 1(d)), one obtains

$$\begin{aligned} &V(0)=R_{\text{load}1}\,i(0) \rightarrow V(0)=-R_{\text{load}1}\,\frac{V_{,x}(0)}{r} \\ &V(L)=R_{\text{load}2}\,i(L) \rightarrow V(L)=-R_{\text{load}2}\,\frac{V_{,x}(L)}{r}. \end{aligned} \tag{18}$$

It is noted that the resistance $R_{\text{load}i}$ or the electrode resistance r can be replaced by any other impedance (e.g., for a resistance-inductance circuit, $R_{\text{load}i}$ has to be replaced by $R_{\text{load}i}+L_{\text{load}i}\,\mathrm{d}/\mathrm{d}t$).

4. Validation of the one-dimensional theory with three-dimensional ANSYS-FE results

In this section, results of our extended beam model are compared to the outcome of 3D FE calculations with ANSYS® 15.0. As a benchmark example, we study a clamped-hinged bimorph with the force load $q_z(x,t)=q_0\cos(\omega t)=25\cos(\omega t)$, see Fig. 2.

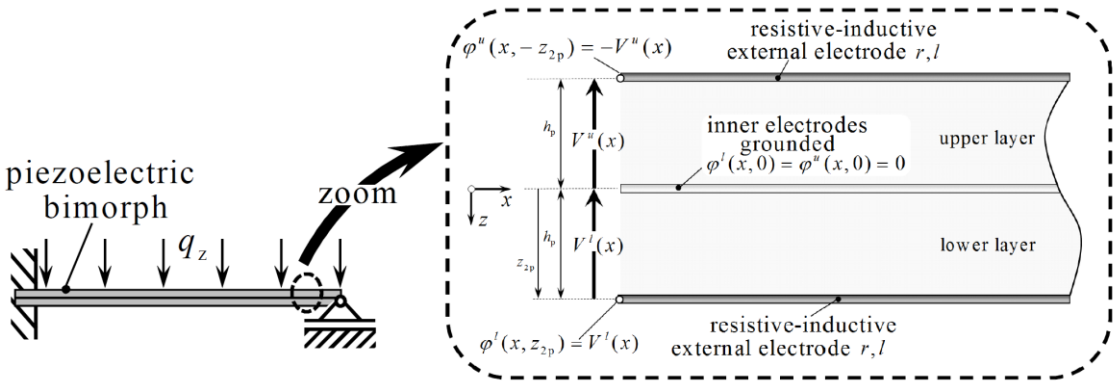

Fig. 2 Clamped-hinged piezoelectric bimorph used in the numerical study.

The parameters are listed in Table 2 of Appendix A and Eq. (A.1) therein. For the electrical boundary conditions, we assume that the electrodes are open-circuited at $x=0$, i.e., $i(0,t)=0$. At $x=L$ the electrodes are linked by the resistance R_{load} and inductance L_{load}, so that the voltage drop is $V(L,t)=R_{\text{load}\,i}\,i(L,t)+L_{\text{load}\,i}\,\mathrm{d}i(L,t)/\mathrm{d}t$. Since we investigate several kinds of electrical loads R_{load}, L_{load} and electrode materials r and l, these values may range from 0 to ∞. The length of the beam is L = 0.04 m, the width b_p =0.004 m and the thickness of one layer $h_p = z_{2\text{p}}$ = 0.0005 m.

The ANSYS® model has $n_x=96$ elements in the axial, ten elements ($n_z=10$) in the thickness and four elements ($n_y=4$) in the width direction. In order to gain more confidence in the accuracy of the FE results, a convergence study concerning the number of elements was conducted, securing that the resulting solution may converge into the exact solution (or at least the difference from the exact one is small). In ANSYS® the SOLID5 eight node brick element is available with DOFs for the displacement field ($u-v-w$) and for the electric potential (V). The ansatz functions for the electrical DOFs are linear, for the displacement field so-called extra shape functions are optionally selected (linear and additional quadratic ansatz functions) to increase the accuracy. For the moderately conductive electrode no proper FE is available. Since the 1D resistance per unit length r and the inductance per unit length l are parameters, the voltage nodes over the electrodes are connected by CIRCU94 elements, which allow for modeling resistances and inductances. For the FE model we assume that the electrode resistance and inductance in the y-direction are negligible. The discrete resistance of the CIRCU94 elements in the x-direction is $R_{\text{d}x}=r(n_y+1)L/n_x$ and the inductance is $L_{\text{d}x}=l(n_y+1)L/n_x$. These values for the electrode impedances are used to connect two neighboring voltage nodes at the conductive electrodes. The same electrical element (CIRCU94) is also used for the terminal circuit. In order to satisfy the grounded electric potential of the inner electrodes, these voltage nodes are prescribed as zero. For the nodes at the clamped end, all mechanical DOFs are locked, whereas the hinge at $x=L$ is realized by locking the displacement in the z-direction: $w(x=L,y,z=0)=0$.

The following parameter variations (cases (a)-(h)) for the electrode properties (r,l) and for the terminal network ($R_{\text{load}}, L_{\text{load}}$) are performed in this study:

- case (a): resistive electrodes $r=11.34\cdot10^{6}\,\Omega/\text{m}, l=0\text{H/m}$ and an attached short circuit $R_{\text{load}}=0\Omega, L_{\text{load}}=0\text{H}$
- case (b): resistive electrodes $r=9.97\cdot10^{6}\,\Omega/\text{m}, l=0\text{H/m}$ and an attached open circuit $R_{\text{load}}\to\infty, L_{\text{load}}=0\text{H}$
- case (c): perfectly conductive electrodes $r=0\Omega/\text{m}, l=0\text{H/m}$ and a resistive network $R_{\text{load}}=18744\Omega, L_{\text{load}}=0\text{H}$
- case (d): resistive-inductive electrodes $r=846.4\cdot10^{3}\,\Omega/\text{m}, l=558.17\text{H/m}$ and an attached open circuit $R_{\text{load}}\to\infty, L_{\text{load}}=0\text{H}$
- case (e): perfectly conductive electrodes $r=0\Omega/\text{m}, l=0\text{H/m}$ and a resistive-inductive

network $R_{\text{load}} = 2328\Omega, L_{\text{load}} = 2.33\text{H}$

- case (f): perfectly conductive electrodes $r = 0\Omega/\text{m}, l = 0\text{H/m}$ and a resistive circuit with $R_{\text{load}} = 3749\Omega, L_{\text{load}} = 0\text{H}$
- case (g): perfectly conductive electrodes $r = 0\Omega/\text{m}, l = 0\text{H/m}$ and an attached inductive circuit with $R_{\text{load}} = 0\Omega, L_{\text{load}} = 4662\text{H}$
- case (h) inductive electrodes $r = 0\Omega/\text{m}, l = 10^6\,\text{H/m}$ and an attached short circuit $R_{\text{load}} = 0\Omega, L_{\text{load}} = 0\text{H}$

First, a frequency analysis is performed (section 4.2) for the cases when the clamped-hinged beam is either

- short-circuited and perfect electrodes ($r = 0\Omega/\text{m}, l = 0\text{H/m}$, $R_{\text{load}} = 0\Omega, L_{\text{load}} = 0\text{H}$) or
- open-circuited and perfect electrodes ($r = 0\Omega/\text{m}, l = 0\text{H/m}$, $R_{\text{load}} \to \infty, L_{\text{load}} = 0\text{H}$) or
- non-electroded ($r \to \infty, l = 0\text{H/m}$, $R_{\text{load}}, L_{\text{load}}$ arbitrary) or
- the terminal network consists of an inductance ($r = 0\Omega/\text{m}, l = 0\text{H/m}$, $R_{\text{load}} = 0\Omega$, $L_{\text{load}} = 2.33\text{H}$) or
- electrodes are inductive ($r = 0\Omega/\text{m}, l = 558.2\text{H/m}$, $R_{\text{load}} = 0\Omega$, $L_{\text{load}} = 0\text{H}$).

For the 3D FE models, only the bending modes in the xy-plane are regarded. Then, the displacement and voltage distributions along the beam length or across the thickness are compared at 10 Hz (quasi-static) and at 7000 Hz (between the second and the third eigenmodes) in section 4.2. The practical application of resistive-inductive electrodes is demonstrated, when the frequency response around the first eigenfrequency is computed for an optimally tuned terminal impedance ($R_{\text{load}}, L_{\text{load}}$) and perfectly conductive electrodes and for resistive-inductive electrodes (r, l) with open- or short-circuited network (section 4.3).

4.1 Natural frequencies

The results of the natural frequency analysis and the relative error between both results are shown in Table 1 (analytical Bernoulli-Euler (BE) vs. 3D FE results with ANSYS®). The relative error is calculated from the eigenfrequencies (EF) as follows

$$\text{relative error} = \frac{\text{EF}_{\text{ANSYS FE}} - \text{EF}_{\text{analytic BE}}}{\text{EF}_{\text{analytic BE}}}. \tag{19}$$

For the ANSYS® results only the bending modes are considered (no torsional, extensional or electrical modes due to inductance or inductive circuit). One sees that the frequencies of the non-electroded beams are the highest, those for the elastic beam (i.e., piezoelectric effects are neglected $\tilde{e}_{31}^{\text{p}} = 0$) are the lowest. The first bending modes computed with ANSYS® are at 1313.2 Hz (non-elec.), 1276.9 Hz (open), 1272.3 Hz (short) and 1255.9 Hz (elastic), whereas the BE-results underestimate these results slightly: 1299.5 Hz (non-elec.), 1266.1 Hz (open), 1260.7 Hz (short) and 1247.4 Hz (elastic). The difference between analytical and 3D-results is in general

lower than 2.26%. When disregarding inductive properties the error is even lower than 1%. Even for the higher modes the 1D theory provides accurate results: e.g. the third mode without electrodes 8786.3 Hz (BE) and 8820.6 Hz (ANSYS®) (rel. error = 0.39%). The difference between the forth mode for the beam without electrodes and the purely elastic beam is $\Delta f = 672\text{Hz}\,(=15013\text{Hz} - 14341\text{Hz})$ and is in good agreement with the analytical results $\Delta f = 701\text{Hz}\,(=15025\text{Hz} - 14324\text{Hz})$.

Table 1 Natural frequencies (Hz) and relative errors (%) of a clamped-hinged beam (Bernoulli-Euler (BE) and ANSYS® FE (bending modes only))

	f_1	f_2	f_3	f_4
Analytic BE $(\tilde{e}_{31} = 0)$	1247.4	4042.8	8434.9	14324
Analytic BE (short)	1260.7	4085.5	8524.2	14577
Analytic BE (open)	1266.1	4090.6	8529.3	14582
Analytic BE (non-electroded)	1299.5	4211.1	8786.3	15025
Analytic BE $(L_{\text{load}} = 2.33\text{H})$	1206.9	1323.4	4091.1	8529.3
Analytic BE $(l = 558.2\text{H/m}, \text{R}_{\text{load}} \to \infty)$	1173.9	1370.1	n.e.*	n.e.*
ANSYS® FE $(\tilde{e}_{31} = 0)$	1255.9	4057.5	8430.8	14341
ANSYS® FE (short)	1272.3	4110.8	8542.8	14534
ANSYS® FE (open)	1276.9	4116.6	8546.6	14541
ANSYS® FE (non-electroded)	1313.2	4243.3	8820.6	15013
ANSYS® FE $(L_{\text{load}} = 2.33\text{H})$	1231.6	1343.0	4117.3	8546.6
ANSYS® FE $(l = 558.2\text{H/m}, \text{R}_{\text{load}} \to \infty)$	1193.7	1401.1	n.e.*	n.e.*
definition of error see Eq. (19)	%	%	%	%
relative error $(\tilde{e}_{31} = 0)$	0.68	0.36	–0.05	0.12
relative error (short)	0.92	0.62	0.22	–0.29
relative error (open)	0.85	0.64	0.20	–0.28
relative error (non-electroded)	1.05	0.76	0.39	–0.08
relative error $(L_{\text{load}} = 2.33\text{H})$	2.05	1.48	0.64	0.20
relative error $(l = 558.2\text{H/m}, \text{R}_{\text{load}} \to \infty)$	1.69	2.26	n.e.*	n.e.*

For the beam configuration with ideal electrodes and an inductive network $L_{\text{load}} = 2.33\text{H}$, the first and second eigenmodes read 1206.9Hz and 1323.4Hz (BE). The electrical mode, which is $f = 1/(2\pi\sqrt{C_{\text{p}} L_{\text{load}}}) = 1271.6\text{Hz}$ for the uncoupled system (i.e., $\tilde{e}_{31}^{\text{p}} = 0$), influences the first bending mode. ANSYS® results are higher, but reflect the same tendency: 1231.6 Hz and 1343.0Hz. Assuming inductive electrodes $l = 558.2\text{H/m}$ and open-circuited electrodes at $x = L$ (i.e., $R_{\text{load}} \to \infty$), an infinite number of electrical eigenmodes exists: for the decoupled system $\tilde{e}_{31}^{\text{p}} = 0$, the first three electrical natural frequencies read $f_{\text{elec}\,k} = k/(2\sqrt{cl}L)$ $= [1290.7\text{Hz}, 2581.5\text{Hz}, 3872.2\text{Hz}]$, see Marshall *et al.* (1996). This formula can be obtained if the eigenvalues of the uncoupled differential Eq. (5) are calculated (i.e., setting $\tilde{e}_{31}^{\text{p}} = 0$) by using the electrical boundary conditions $V_{,x}(0) = V_{,x}(L) = 0$. We only list the first two modes, which are overestimated by the ANSYS model: 1193.7Hz and 1401.1Hz (ANSYS) in comparison to 1173.9Hz (BE) and 1370.1Hz (BE), yielding the relative errors = 1.69% and 2.26%.

4.2 Harmonic frequency responses (10 Hz and 7000 Hz)

The harmonic frequency responses for the deflection and voltage distributions are shown in Figs. 3 and 4. The excitation in the quasi-static regime (Fig. 3–10Hz) shows the beam deflection $\hat{w}_0(x)$ and voltage distributions along the external electrode $\hat{V}(x) = \hat{\phi}(x, z_{2\text{p}})$, see Eq. (6). As expected, the elastic beam shows the largest deflections (0.0169 mm for BE and 0.0165 mm for ANSYS®). In case of no electrodes the deflection is 8% less for both the analytical and the numerical ANSYS® results $\hat{w}_0(x)$ = 0.0156 mm and 0.0151 mm at $x \approx 0.023\text{m}$). In case of highly conductive electrodes ($r \to 0$, Fig. 3 bottom), the potential must be uniformly distributed along the layer electrodes. This is true for open-circuits (gray) and for an inductive terminal circuit $L_{\text{load}} = 4662\text{H}$ (gray-dash-dot): the electric potential is -2.30V and 0.31V (ANSYS®) and agrees with the analytical results -2.44V and 0.35V.

These results can be verified as follows: by assuming ideal electrodes $r \to 0$, the solution for the voltage yields, see (7)

$$V(x) = C_1 x + C_0 \tag{20}$$

Due to the open circuit condition at the left end ($i(0) = 0 \to V_{,x}(0) = 0$) the constant C_1 vanishes, meaning that the equipotential area condition is fulfilled over the electrodes. From Kirchhoff's voltage rule for the inductive network $L_{\text{load}}\text{d}i(L)/\text{d}t = V(L)$ follows (in the frequency domain)

$$L_{load}\left(\int_0^L \hat{i}_{,x}(x)dx - \hat{i}(0)\right)\mathbf{i}\omega = \hat{V}(L) \tag{21}$$

Inserting Eq. (8) into Eq. (21) and considering the boundary condition $\hat{w}_{0,x}(0) = 0$ one finds for the inductive circuit

$$\hat{V}_{\text{ind.}} = -\frac{\tilde{e}_{31}^{\text{p}} b_{\text{p}} z_{\text{mp}}}{C_{\text{p}}\left(1-\dfrac{1}{C_{\text{p}} L_{\text{end}} \omega^2}\right)} \hat{w}_{0,x}(L) = 0.35\text{V}. \tag{22}$$

For the open circuit (i.e. $L_{\text{load}} \to \infty$) one finds

$$\hat{V}_{\text{open}} = -\frac{\tilde{e}_{31}^{\text{p}} b_{\text{p}} z_{\text{mp}}}{C_{\text{p}}} \hat{w}_{0,x}(L) = -2.44\text{V}. \tag{23}$$

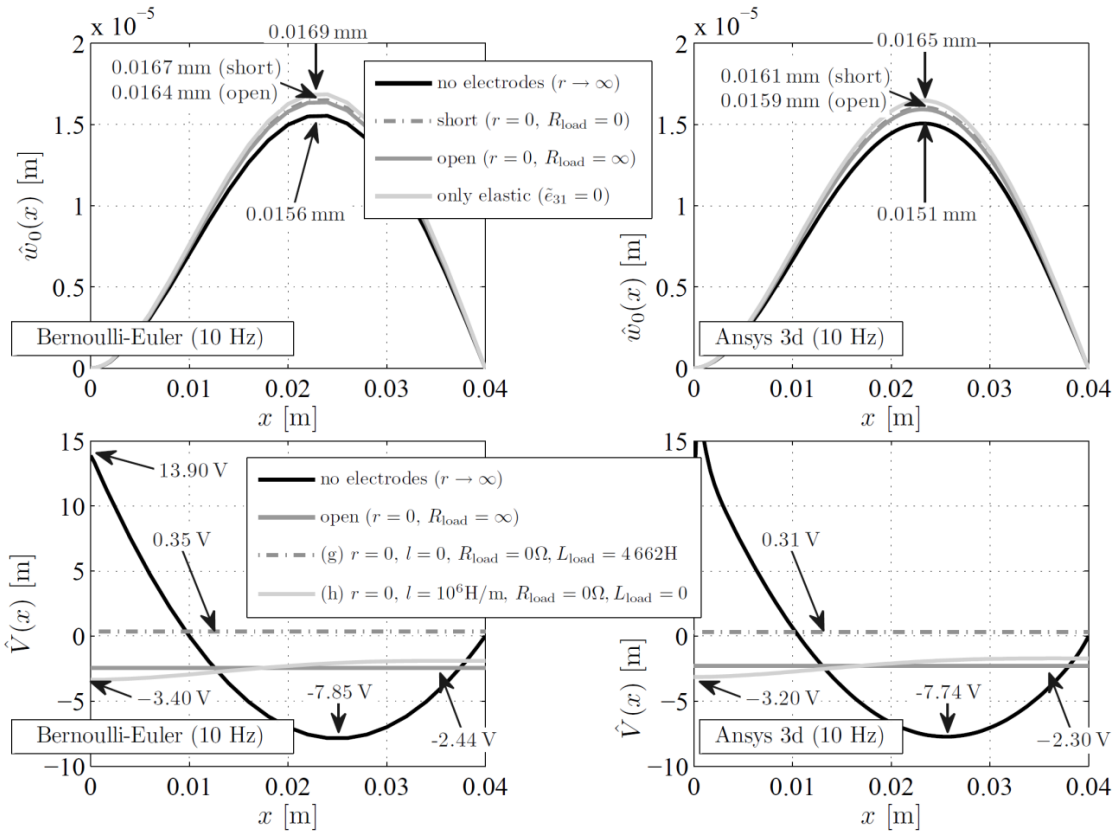

Fig. 3 Lateral deflection $\hat{w}_0(x)$ (above) and voltage across the electrodes $\hat{V}(x)$ along the beam axis (bottom) at $f = 10\text{Hz}$ for the BE- (left) and the ANSYS model (right)

One notices that $\hat{V}_{\text{ind.}}$ is frequency-dependent and converges to the open-circuit voltage for large frequencies ω. When the piezoelectric layers are not covered by electrodes ($r \to \infty$, black), it can be shown that dividing Eq. (5) by r, then taking the limit $r \to \infty$, the voltage distribution is proportional to the curvature of the beam

$$\hat{V}_{\text{non elec.}}(x) = -\frac{\tilde{e}_{31}^{\text{p}} b_{\text{p}} z_{\text{mp}}}{c} \hat{w}_{0,xx}(x). \tag{24}$$

For $x = 0$ one finds $\hat{V}_{\text{non elec.}}(0) = 13.90\text{V}$. A similar shape of this curve is obtained by the FE model, which deviates from the analytical result only close to the clamped end due to the edge effect. When the excitation frequency is increased (7000 Hz–between the second and the third mode), the lateral deflection and the through-the-thickness potential distribution are shown in Fig. 4. The short- and open-circuited displacements are almost the same and very close to the result, where the electrodes are linked by the resistance $R_{\text{load}} = 3749\Omega$ (case (f)-light gray curve).

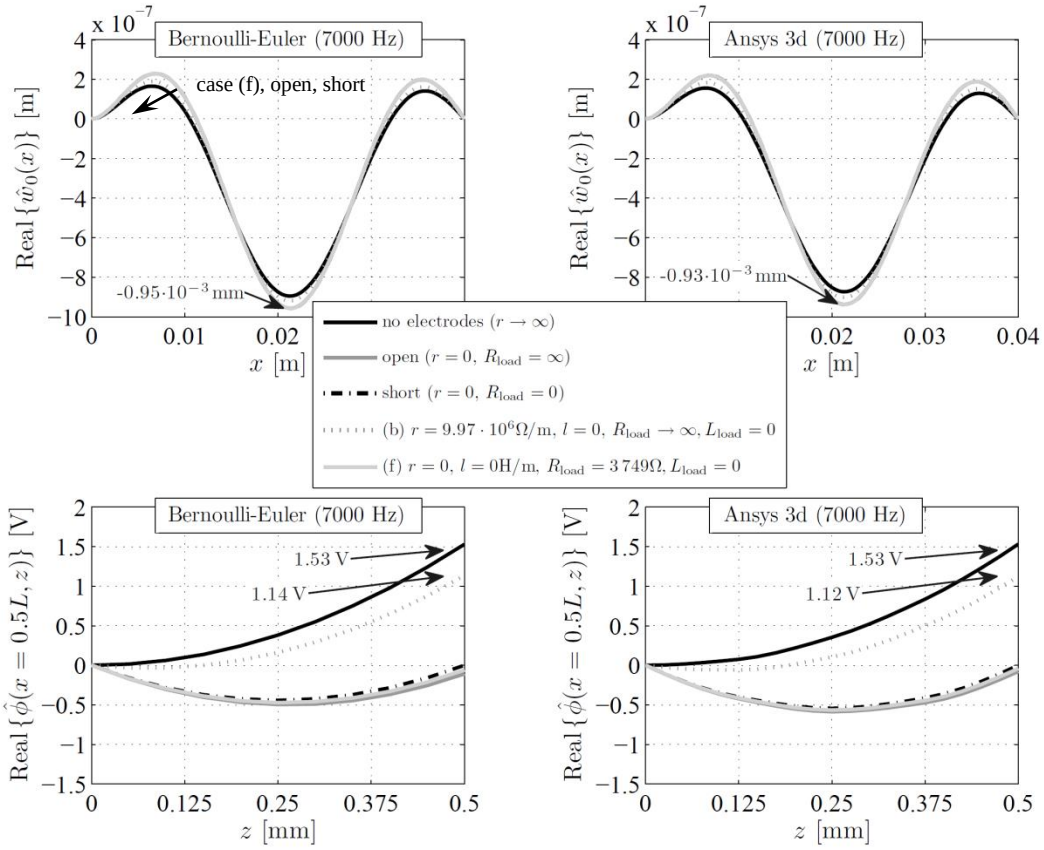

Fig. 4 Lateral deflection $\hat{w}_0(x)$ (above) along the beam axis and potential distribution along the thickness of the layer $\hat{\phi}(0.5L, z)$ (bottom) at $f = 7000\text{Hz}$ for the BE- (left) and the ANSYS model (right)

Differences to the configuration without electrodes (black) and the one with resistive electrodes ($r = 9.97 \cdot 10^6 \Omega/\mathrm{m}$, gray-dashed) are close the same for the analytical and FE results (e.g. the displacements at $x = 0.02\mathrm{m}$ are $-0.95 \cdot 10^{-3}\mathrm{mm}$ for BE and $-0.93 \cdot 10^{-3}\mathrm{mm}$ for ANSYS®: relative error 2.2%). The potential distribution at the half of the beam length $\hat{\phi}(0.5L, z)$ (Fig. 4 bottom) shows the nonlinear distribution with respect to the thickness. In a first approximation, the exact solution within the Bernoulli-Euler framework yields a linear and a quadratic part, where the latter one is the influence due to the bending strain, see Eq. (6). In general, the ANSYS results match quite well with the analytical results. The voltage, when electrodes are not present ($r \to \infty$), is $\mathrm{Real}\{\hat{V}(0.5L)\} = 1.53\mathrm{V}$ at $z = 0.5\mathrm{mm}$ for both models. For resistive electrodes (case (b)) the voltage is $\mathrm{Real}\{\hat{V}(0.5L)\} = 1.14\mathrm{V}$ for BE and $\mathrm{Real}\{\hat{V}(0.5L)\} = 1.12\mathrm{V}$ for ANSYS® (relative error of 1.79%).

4.3 Passive vibration control

In this subsection, we focus on the practical use of the optimal material properties of the electrodes. We show that the damping effect by means of the electrodes is much more efficient than damping by a simple attached circuit. Figs. 5 and 6 show the frequency response around the first eigenfrequency and the transient response due to the impulse load $q_z(x,t) = q_0 \delta(t)$.

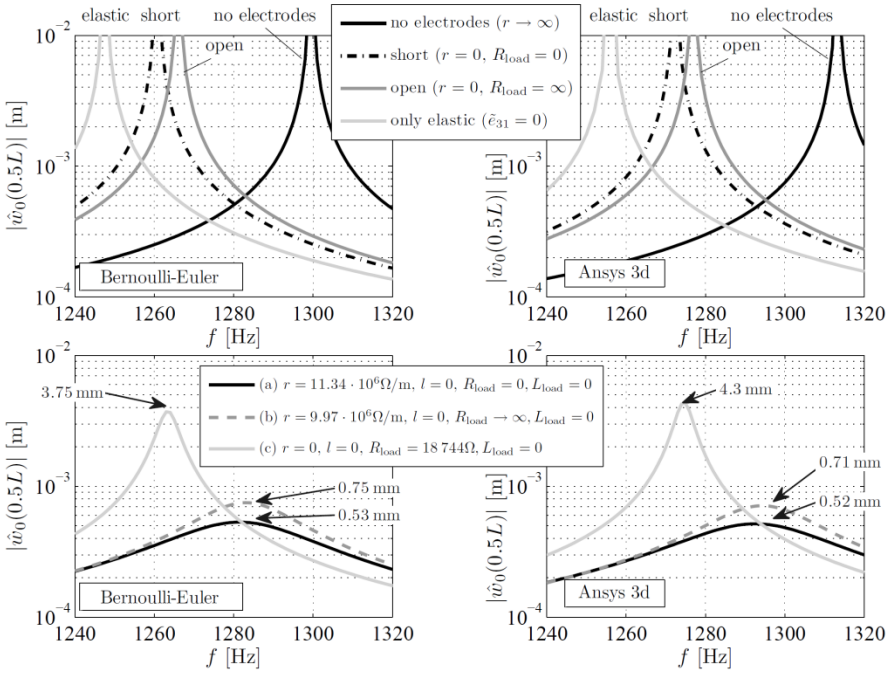

Fig. 5 Frequency response $|\hat{w}_0(0.5L)|$ around the first eigenfrequency (above: elastic, short, open, no electrodes; bottom: optimal resistive electrodes with attached short (case (a)) and open circuit (case (b)) and optimal terminal resistance (case (c))

Fig. 5 shows the frequency response for the limit cases (above: elastic, short, open, no electrodes) and for the optimally tuned circuits (bottom: case (a) optimal resistive electrode with the terminal short circuited, case (b) optimal resistive electrode with open circuit, case (c) ideal electrodes with optimal terminal resistance). The first eigenfrequencies for the short- and the open-circuited beam are 1260.7 Hz and 1266.1 Hz (BE), see also Table 1. The points, where these two curves intersect, correspond to the maximum displacement $|\hat{w}_0(0.5L)| = 3.75\text{mm}$ for case (c): if the attached circuit resistance is optimized $R_{\text{load}} = R_{\text{opt}} = 18744\Omega$, the lowest possible deflection may be obtained at $f = 1263.4\text{Hz}$. If the electrodes are properly tuned, then the amplitudes are lower: electrodes with $r = 11.34 \cdot 10^6 \Omega/\text{m}$ and $R_{\text{load}} = 0$ (case (a) black solid) yield a displacement of only 0.53 mm (reduction of -86%). If the electrodes are open-circuited, one finds 0.75 mm (case (b) gray dashdot, -80%). These results correspond with ANSYS® results, which are 0.52 mm and 0.71 mm, respectively: the relative errors between BE and ANSYS® are 2.0% (case (a)) and 5.6% (case (b)).

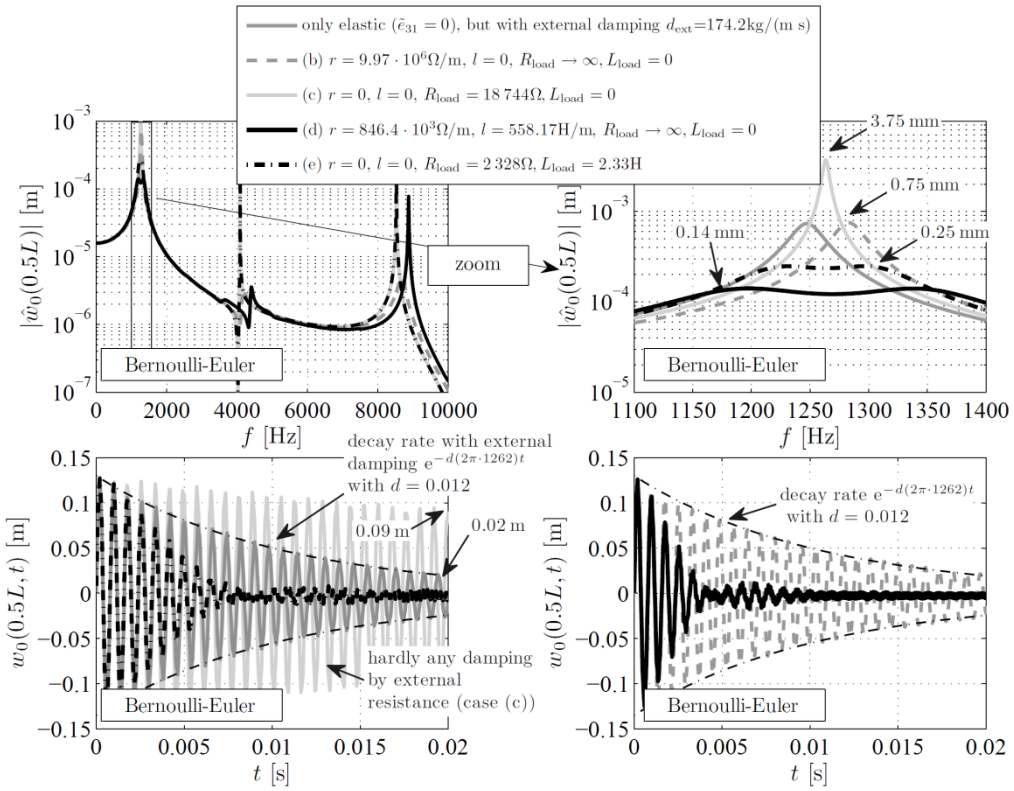

Fig. 6 Frequency response $|\hat{w}_0(0.5L)|$ around the first eigenfrequency and transient response $w_0(0.5L,t)$ (elastic with mechanical damping, optimal resistance and resistive electrode, optimal RL -values for terminal circuit and optimal rl -values for electrodes (above); transient response due to impulse load (bottom))

As already known from literature (e.g., Schoeftner and Irschik (2011b)), the damping performance can be further enhanced by using resistive-inductive networks. The major drawback of that kind of systems is their high sensitivity concerning parameter uncertainties. In addition to the previously discussed optimized resistive electrodes (cases (b) and (c)), the frequency response is shown in Fig. 6, when the resistive-inductive terminal load (case (e) black dashdot) and the rl-electrode properties (case (d) black) are optimized. The two peaks at 1173.9 Hz and 1370.1 Hz (see Table 1 for the electrically undamped system) are attenuated. The highest deflection for the rl-optimized electrodes is $|\hat{w}_0(0.5L)| = 0.14\text{mm}$ (black solid), for the RL-optimized circuit it is 0.25mm (black dashdot).

Furthermore, the transient response due to the impact load $q_z(x,t) = q_0\delta(t)$ is shown at the bottom of Fig. 6. The optimally tuned resistive circuit (case (c) light gray dashed) hardly contributes damping (at $t = 0.02\text{s}$ the deflection amplitude is still 0.09 mm) in comparison to the beam with the optimal electrode resistance and attached open circuit (case (b) gray dashdot): the deflection amplitude is 0.02 m at $t = 0.02\text{s}$. This is the same output as if we add external damping to the beam equation with d_{ext} = 174.2 kg/(ms) corresponding to a logarithmic damping of $d = 0.012$ (exponential decaying envelope). When the RL-circuit is optimally tuned (black dashdot), amplitudes are almost vanished at $t = 0.008\text{s}$. For the optimal choice of rl (black solid), most of the amplitudes are significantly reduced at $t = 0.0045\text{s}$. Hence, this result reveals the importance of the proper electrode characteristics, which will be further investigated in a future contribution.

5. Conclusions

In this contribution, a 1D theory for smart piezoelectric beams is presented which considers the presence of finite conductivity of the electrodes. Contrary to the actual state of the art, where the potential over the electrodes of piezoelectric layers is evenly distributed, we investigate the coupling of non-ideal moderately conductive electrodes with the mechanical deformation of a slender beam. The outcomes of our beam theory are two coupled differential equations: the Bernoulli-Euler equation is extended by a voltage-dependent term and is coupled to the Telegrapher's equation for the electric potential. Our derived 1D equations results are compared to those from 3D FE analysis in ANSYS®. A natural frequency analysis is performed and frequency responses for the lateral displacement and the electrode voltage are computed. A good agreement with the 3D numerical results is obtained. Finally, the practical relevance of this type of electrodes is pointed out. It is shown that properly tuned resistive-inductive electrodes provide a huge potential for passive vibration control: vibrations are much more attenuated compared to optimized resistive electrodes or to an optimally attached resistive-inductive circuit.

Acknowledgments

J. Schoeftner acknowledges support from the Austrian Science Fund FWF via the project P 26762-N30 and A. Benjeddou (SUPMECA), G. Buchberger (Institute of Biomedical Mechatronics) from the K2-Comet Linz Center of Mechatronics LCM (projects: C220101, C250103).

References

Benjeddou, A., Trindade, M. A. and Ohayon, R. (1997), "A unified beam finite element model for extension and shear piezoelectric actuation mechanisms", *J. Intel. Mat. Syst. Struct.*, **8**(12), 1012-1025.

Benjeddou, A., Trindade, M.A. and Ohayon, R. (1999), "New shear actuated smart structure beam finite element", *AIAA J.*, **37**(3), 378-383.

Buchberger, G. and Schoeftner, J. (2013), "Modeling of slender laminated piezoelastic beams with resistive electrodes – comparison of analytical results with three-dimensional finite element calculations", *Smart Mater. Struct.*, **22**(3), 032001 (13pages).

Buchberger, G., Schwoediauer, R., Arnold, N. and Bauer, S. (2008b), "Cellular ferroelectrets for flexible touchpads, keyboards and tactile sensors", *IEEE Sensors Conference Proceedings* 2008, **10**, 1520-1523.

Buchberger, G., Schwoediauer, R. and Bauer, S. (2008), "Flexible large area ferroelectret sensors for location sensitive touchpads", *Appl. Phys. Lett.*, **92**(12), 123511 (3 pages).

Chopra, I. (2002), "Review of the state of art of smart structures and integrated systems", *AIAA J.*, **40**(11), 2145-2187.

Crawley, E.F. (1994), "Intelligent structures for aerospace: a technology overview and assessment", *AIAA J.*, **32**(8), 1689-1699.

Forward, R.L. (1979), "Electronic damping of vibrations in optical structures", *Appl. Opt.*, **18**(5), 670-677.

Hagood, N. W. and von Flotow, A. (1991), "Damping of structural vibrations with piezoelectric materials and passive electrical networks", *J. Sound Vib.*, **146**(2), 243-268.

Janocha, H., (2007), *Adaptronics and smart structures: basics, materials, design, and application*, Berlin, Springer.

Krommer, M. and Irschik, H. (1999), "On the influence of the electric field on free transverse vibrations of smart beams", *Smart Mater. Struct.*, **8**(3), 401-410.

Krommer, M. (2001), "On the correction of the Bernoulli-Euler beam theory for smart piezoelectric beams", *Smart Mater. Struct.*, **10**(4), 668-680.

Krommer, M. and Irschik, H. (2002), "An electromechanically coupled theory for piezoelastic beams taking into account the charge equation of electrostatics", *Acta Mech.*, **154**(1), 141-158.

Lediaev, L. (2010), "Finite element modeling of piezoelectric bimorphs with conductive polymer electrodes", doctoral thesis Montana State University, Bozeman, Montana.

Marshall, S.V., DuBroff, R.E. and Skitek, G.G. (1996), *Electromagnetic Concepts & Applications*, (4th Ed.), Prentice-Hall, Upper Saddle River New Jersey.

Moheimani, S.O.R. and Fleming, A.J. (2006), *Piezoelectric Transducers for Vibration Control and Damping*, Dordrecht, Springer.

Niederberger, D., Fleming, A., Moheimani, S.O.R. and Morari, M. (2004), "Adaptive multi-mode resonant piezoelectric shunt damping", *Smart Mater. Struct.*, **13**(5), 1025-1035.

Park, C.H. (2003), "Dynamics modelling of beams with shunted piezoelectric elements", *J. Sound Vib.*, **268**(1), 115-129.

Preumont, A. (2006), *Mechatronics Dynamics of Electromechanical and Piezoelectric Systems*, Dordrecht, Springer.

Schoeftner, J. and Buchberger, G. (2013), "Verfahren zur Aenderung des statischen und/oder dynamischen Istverhaltens eines insbesondere elastischen Koerpers unter ausserer Belastung", Patent 513259, filed January 29th 2013 and issued March 15th, 2014.

Schoeftner, J., Buchberger, G. and Benjeddou, A. (2015), "Slender piezoelectric beams with resistive-inductive electrodes – modeling and axial wave propagation" (submitted simultaneously for publication in *Smart Struct. Syst.* 2016)

Schoeftner, J., Buchberger, G., Brandl, A. and Irschik, H. (2015b), "Theoretical prediction and experimental verification of shape control of beams with piezoelectric patches and resistive circuits", *Compos. Struct.*, **133**, 746-755.

Schoeftner, J., Buchberger, G. and Irschik, H. (2014), "Static and dynamic shape control of slender beams by piezoelectric actuation and resistive electrodes", *Compos. Struct.*, **111**, 66-74.

Schoeftner, J. and Irschik, H. (2011), "A comparative study of smart passive piezoelectric structures interacting with electric networks: Timoshenko beam theory versus finite element plane stress calculations", *Smart Mater. Struct.*, **20**(2), 025007 (13 pages).

Schoeftner, J. and Irschik, H. (2011b), "Passive shape control of force-induced harmonic lateral vibrations for laminated piezoelastic Bernoulli-Euler beams–theory and practical relevance", *Smart Struct. Syst.*, **7**(5), 417-432.

Thornburgh, R.P. and Chattopadhay, A. (2002), "Simultaneous modeling of mechanical and electrical response of smart composite structures", *AIAA J.*, **40**(8), 1603-10**.**

Thornburgh, R.P. and Chattopadhay, A. (2003), "Modeling and optimization of passively damped adaptive composite structures", *J. Intel. Mater. Syst. Struct.*, **14**(4-5), 247-56.

Trindade, M.A. and Maio, C.E.B. (2008), "Multimodal passive vibration control of sandwich beams with shunted shear piezoelectric materials", *Smart Mater. Struct.*, **17**(5), 055015 (10 pages).

Tzou, H. S. (1998), "Multifield transducers, devices, mechatronic systems and structronic systems with smart materials", *Shock Vib. Dig.*, **30**(4), 282-294.

FC

Appendix A

The material properties for the piezoelectric transducers used in our study read:

• Density $(\mathrm{kg/m^3})$: $\rho = 7750$

• Elasticity components in Voigt notation $(\mathrm{N/m^2})$: $C_{11} = C_{22} = 121.00 \cdot 10^9$, $C_{12} = 75.40 \cdot 10^9$, $C_{13} = C_{23} = 75.20 \cdot 10^9$, $C_{33} = 111.00 \cdot 10^9$, $C_{44} = C_{55} = 21.10 \cdot 10^9$, $C_{66} = \left(C_{11} - C_{12}\right)/2 = 22.80 \cdot 10^9$, remaining components $C_{ij} = 0$

• Piezoelectric components in Voigt notation $(\mathrm{C/m^2})$: $e_{31} = e_{32} = -5.40$, $e_{33} = 15.80$, $e_{24} = e_{15} = 12.30$, remaining components $e_{ij} = 0$

• Permittivity components in Voigt notation: $\kappa_{11} = \kappa_{22} = 1649\varepsilon_0$, $\kappa_{33} = 1750\varepsilon_0$, $\varepsilon_0 = 8.854 \cdot 10^{-12}\,\mathrm{C/(Vm)}$, remaining components $\kappa_{ij} = 0$

Based on these values, the effective constants (reduced axial stiffness $\tilde{C}_{11}^{\mathrm{p}}$, stress piezoelectric coupling constant $\tilde{e}_{31}^{\mathrm{p}}$ and blocked strain-free permittivity $\tilde{\kappa}_{33}^{\mathrm{p}}$, see Buchberger and Schoeftner (2013) for their derivation). Further data for the numerical example can be found in Table 2.

Table 2 Parameters for the numerical example

variable (unit)	Value
$\rho_{\mathrm{p}}\,(\mathrm{kg/m^3})$	7750
$z_{1\mathrm{p}}\,(\mathrm{m})$	0
$z_{2\mathrm{p}}\,(\mathrm{m})$	$5.00 \cdot 10^{-4}$
$b_{\mathrm{p}}\,(\mathrm{m})$	$4.00 \cdot 10^{-3}$
$L\,(\mathrm{m})$	$4.00 \cdot 10^{-2}$
$\tilde{e}_{31}^{\mathrm{p}}\,(\mathrm{As/m^2})$	−10.48
$\tilde{\kappa}_{33}^{\mathrm{p}}\,(\mathrm{As/V/m})$	$2.10 \cdot 10^{-8}$
$\tilde{C}_{11}^{\mathrm{p}}\,(\mathrm{N/m^2})$	$6.15 \cdot 10^{10}$
$q_0\,(\mathrm{N/m})$	25

The layer thickness h_{p}, the mean distance to the x-axis z_{mp}, the mass per unit length M_u, the longitudinal stiffness K_{N}, the bending stiffness K_{M}, the capacity per unit length c and the capacity of the electrodes C_{p} read

$$
\begin{aligned}
&h_{\mathrm{p}} = z_{2\mathrm{p}} - z_{1\mathrm{p}} = 5.00{\cdot}10^{-4}\,\mathrm{m}\\
&z_{m\mathrm{p}} = \frac{z_{2\mathrm{p}} + z_{1\mathrm{p}}}{2} = 2.50{\cdot}10^{-4}\,\mathrm{m}\\
&M_{w} = M_{u} = 2\rho_{\mathrm{p}} b_{\mathrm{p}} h_{\mathrm{p}} = 3.10{\cdot}10^{-2}\,\mathrm{kgm}^{-1}\\
&K_{\mathrm{N}} = 2\tilde{C}_{11}^{\mathrm{p}} b_{\mathrm{p}} h_{\mathrm{p}} = 246.07{\cdot}10^{3}\,\mathrm{N}\\
&K_{\mathrm{M}} = \frac{2}{3}\tilde{C}_{11}^{\mathrm{p}} b_{\mathrm{p}}\left(z_{2\mathrm{p}}^{3} - z_{1\mathrm{p}}^{3}\right) + \frac{\tilde{e}_{31}^{2\mathrm{p}}\left(z_{2\mathrm{p}} - z_{1\mathrm{p}}\right)^{3} b_{\mathrm{p}}}{6\tilde{\kappa}_{33}^{\mathrm{p}}} = 20.95{\cdot}10^{-3}\,\mathrm{Nm}^{2}\\
&c = \tilde{\kappa}_{33}^{\mathrm{p}} b_{\mathrm{p}} / h_{\mathrm{p}} = 168.02{\cdot}10^{-9}\,\mathrm{AsV}^{-1}\mathrm{m}^{-1}\\
&C_{\mathrm{p}} = cL = 6.72{\cdot}10^{-9}\,\mathrm{AsV}^{-1}.
\end{aligned}
\tag{A.1}
$$